# Measurements and Performance of a Microstrip Beam Probe System

J. D. Gilpatrick, K. F. Johnson, S. Lloyd, D. Martinez, R. Meyer, G. Neuschaefer, J. Power, R. B. Shurter, and F. D. Wells
Los Alamos National Laboratory, Los Alamos, NM 87545

## *Abstract*

Microstrip probes and associated processing electronics have been designed and used to measure charged-beam position, angle, intensity, output phase, and energy. As a bunched, charged beam periodically passes through a microstrip probe, a bipolar signal proportional to the beam's current and position is induced into each of the probe's four axial symmetric lobes. Processing electronics and computer algorithms transform two probe signals into beam intensity and into centroids of the six-dimensional, phase-space beam distributions. These beam centroids can then be plotted with cavity data so that output beam characteristics can be expressed as a function of cavity power and phase. This paper will describe the system, and discuss typical beam/cavity interaction data, measurement errors, and system performance.

## I. THE MICROSTRIP SYSTEM

The microstrip systems consist of three components: the microstrip probe, the processing electronics, and the computer hardware and software that provide experimenters with beam information. This section will concentrate primarily on the first two items, and the measurement algorithms.

The microstrip probe is a short version of typical directional coupler probes [1]. These noninterceptive, electromagnetic beam probes consist of four symmetrically-placed lobes that sense the bunched-beam image currents. Stripline transmission lines are attached to the front and back of each microstrip transmission-line lobe. As the beam image currents pass through the probe, periodic bipolar signals are launched to both the downstream termination, via the stripline, and the processing electronics, via the upstream transmission line. Table I shows the key parameters of these probes as well as the expected signal power of the 425-MHz frequency component [2].

**Table I. Installed Probe Geometries and Signal Powers**

| Probe Bore (mm) | Lobe Subtended Angle (Radians) | Lobe Length (mm) | Overall Probe Length (mm) | Signal Power 10mA, 5 MeV Beam (dBm) |
|---|---|---|---|---|
| 45 | π/4 | 2.25 | 12.7 | -34 |
| 16 | π/4 | 2.25 | 8.2 | -33 |
| 10 | π/4 | 6.13 | 11.3 | -30 |

The electrical characterization of the probe must provide a measure of position sensitivity and offset, phase delay through the probe, and beam coupling for the bunched beam. The first two items are measured with an automated, movable-wire test fixture [3] that calculates the centered-beam-position sensitivity and offset. The phase delay and beam coupling are measured using a coaxial, transmission-line test fixture and network analyzer. Measured position sensitivities range from 4.5 dB/mm to 1.2 dB/mm and offsets are $< \pm 0.15$ mm. Coupling between the probe lobe and the center conductor of the test fixture is typically -37 to -40 dB, and probe phase delays are 12.8 radians at 425 MHz.

The processing electronics consist of three modules [4]. A down-converter module converts the bunched-beam 425-MHz radio-frequency (RF) signals from the microstrip probe, and an accelerating-cavity field-monitor signal, to intermediate frequency (IF) signals of 20 MHz. This conversion improves the accuracy of the IF processing electronics and decreases the component costs. After the signals are down-converted, they are appropriately divided, phase-matched, and fed to the other two modules: a position and intensity module, and an output-phase and time-of-flight (TOF) module.

The position and intensity module comprises a position circuit and an intensity circuit. The position circuit uses the amplitude-to-phase conversion technique [5] to transform the IF lobe signals to an output voltage that is a function of beam position. The intensity circuit synchronously detects the amplitude of the converted and summed four-lobe signals. The third module, output-phase and TOF circuitry, compares the phases of two sets of signals using two digital phase detectors. For the beam output phase, the converted cavity-field sample is compared with the converted and summed probe-lobe signals; the output signal is proportional to the phase between these signals. The TOF circuitry compares the summed and converted signals from two different probes having a known separation along the beamline. This output is proportional to the flight time of the last partial βλ distance of a bunch traveling between the two probes.

For each of the output signals, algorithms transform, linearize, and calculate the final measured values. The horizontal- and vertical-position output-signal nonlinearities are corrected in the digitizing computer software. Equations 1 and 2 are the corrections for the nonlinearities in the microstrip probe and position-processing electronics, respectively.

$$\bar{x} = x_0 + S_x R_{\bar{x}} - 1.797\text{X}10^{-4} R_{\bar{x}}^2 - 1.412\text{X}10^{-4} R_{\bar{x}}^3 \qquad (1)$$

and

$$R_{\bar{x}} = 20 \log \left[ \tan \left( \left( \frac{\pi}{1.5 A V_{RF}} \right) V + \frac{\pi}{4} \right) \right] , \qquad (2)$$

where $R_{\bar{x}}$ is the nonlinear correction of the position-processing electronics, $\bar{x}$ is the beam position, V is the signal from the microstrip processing electronics, A and $V_{RF}$ are gain and circuit signal constants, and $x_0$ and $S_x$ are the measured probe-position offset and sensitivity. The beam angle is also calculated if there is a drift between two probes.

*Work supported and funded by the US Department of Defense, Army Strategic Defense Command, under the auspices of the US Department of Energy.

0-7803-0135-8/91$01.00 ©IEEE

The intensity output signal is transformed from volts to milliamperes of beam current by a conversion factor of 10 to 20 mA per volt [2].

The TOF signal is transformed to flight time, normalized beam velocity, and finally, beam energy [6].

$$\overline{W} = M_0c^2\left[\left(1-\left(\frac{dw}{c\left(n_wT+\frac{T}{T_{IF}}\tau_{IF}\right)}\right)^2\right)^{-\frac{1}{2}}-1\right] , \qquad (3)$$

where $\overline{W}$ is the mean beam energy, $\tau_{IF}$ is the flight time of the last partial $\beta\lambda$ distance of a bunch traveling a distance $dw$, $n_w$ is the integer number of $\beta\lambda$s in distance $dw$, T and $T_{IF}$ are the bunching and IF periods, and $M_0c^2$ is the beam's rest energy. The output beam phase with respect to an upstream cavity is calculated using the phase difference between the probe signal and a cavity-field monitor loop signal. The correction for beam phase changes due to beam energy changes during the drift is shown in Equation 4.

$$\overline{\phi} = \phi_s - \left(\frac{d_\phi}{\beta\lambda_0} - n_\phi\right)2\pi , \qquad (4)$$

where $\overline{\phi}$ is the average output phase of the beam, $\phi_s$ is the phase recorded by the processing electronics, $\lambda_0$ is the free-space bunching wavelength, and $n_\phi$ is the number of integer $\beta\lambda$s in $d_\phi$ (the distance between an RF cavity reference-plane and a microstrip probe).

## II. Beam/Cavity Interaction Measurements

Because beam output phase and energy are measured as well as beam position and intensity, the interaction between the accelerating cavity and its output beam can be determined. The linac RF-field phase and amplitude can be determined by measuring the beam's energy, output phase, and transmission efficiency. These data are then compared with single-particle simulations as generated by particle and ray-tracing simulation codes (e.g., PARMILA, TRACE).

At Los Alamos, these graphical studies describing the output beam as a function of two independent variables are known as phase scans. Phase scans plot output beam current, intensity, phase, and energy as a function of the two independent variables, cavity (or input-beam) phase and cavity power (or gap voltage). A fourth plot, output beam energy as a function of output beam phase, is shown in Figure 1 for a 5-MeV, $H^-$ linac. Each of the "pin wheel" loci corresponds to single-particle simulations for a particular cavity power level or gap voltage. The 206-kW data show that the linac gap voltage was 8% higher than the 1.00 x design gap voltage [7]. A semiautomated version of these scans has been implemented on the drift-tube linac, providing data acquisition and analysis within a few minutes.

Transmission scans are a specific subset of the general beam/cavity measurements used to determine the RF power set points for a Radio-Frequency Quadrupole (RFQ). Beamtransmission efficiency, output beam current, intensity, phase, and energy are calculated and displayed as a function of

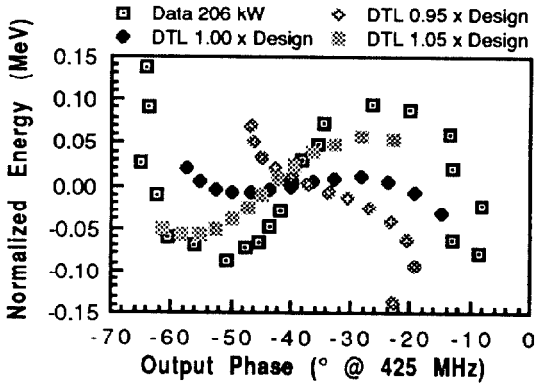


Figure 1. DTL Beam Energy vs Beam Output Phase.

power inside the cavity. To compare data with simulations (e.g., using PARMTEQ), transmission scans are expressed in terms of the RFQ vane voltage (Figure 2). The transmission is different from the theoretical design because the

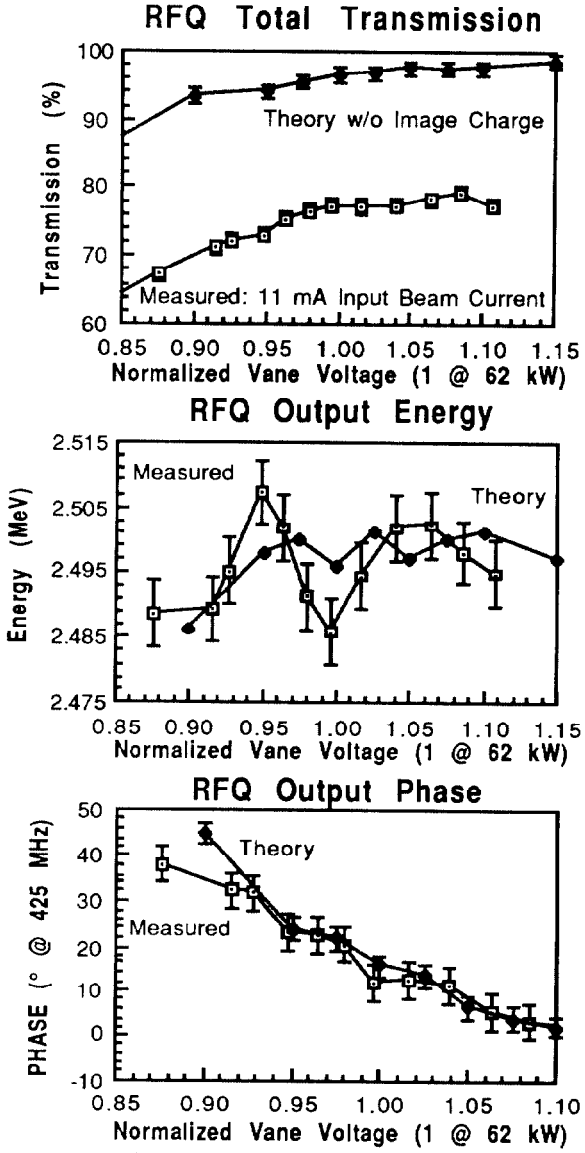


Figure 2. Transmission Scan

input beam was not properly positioned entering the RFQ, and image currents were not included in the simulations.

## III. MEASUREMENT ERRORS

There are two types of measurement errors: fundamental and systematic. Fundamental errors are errors that cannot be reduced because of natural laws of physics; these limit both the measurement resolution and accuracy. Examples are thermal and shot noise. Systematic errors are errors that limit accuracies but do not limit resolution of the measurements. Examples are transverse probe-alignment errors with respect to the beamline (which affect the absolute beam position accuracy).

**Table II. Measurement Errors and Uncertainties**

| Beam Variable | Error | Upper Limits (% Full Range) |
|---|---|---|
| *Fundamental Errors (Accuracy & Resolution)* | | |
| Energy**/Phase | Thermal Noise* | ± 0.002/± 0.02 |
| | Electronic Noise | ± 0.014/± 0.3 |
| | RFI (-34 dBc) | ± 0.03/± 0.6 |
| Intensity | Thermal/Shot Noise* | ± 0.004 |
| | Probe/Beam Coupling | ± 5 |
| | Electronic Noise | ± 0.14 |
| | RFI (-34 dBc) | ± 2 |
| Position | Thermal Noise* | ± 0.05 |
| | Electronic Noise | ± 0.3 |
| | RFI (-34 dBc) | ± 0.5 |
| *Systematic Errors (Accuracy)* | | |
| Energy**/Phase | Cable Delays | ±0.08/± 2.3 |
| | Probe Alignment | ± 0.021/± 0.09 |
| | Electronic Drift | ± 0.024/± 0.3 |
| | Probe/Elect. Match | ± 0.19/± 2.2 |
| Intensity | Cable Losses | ± 1 |
| | Electronic Drift | ± 0.2 |
| | Probe/Elect. Match | ± 3.5 |
| Position | Cable Losses & Delays | ± 0.14 |
| | Probe Alignment | ± 1.0 |
| | Electronic Drift | ± 0.5 |
| | Probe/Elect. Match | ± 1.0 |

* Noise limits assume a 1-MHz bandwidth to the electronics and a 40-dB electronic signal-to-noise ratio.
** The energy measurement errors are based on a flight path length of 12 $\beta\lambda$ at nominal beam energy.

The time and flight path uncertainty relationship can be calculated by differentiating Equation 3. The measured beam-energy resolution or accuracy, $\Delta W$, is expressed as

$$\Delta W = \frac{(\beta\gamma)^3 M_0 c^2 c \Delta\tau}{dw} , \qquad (5)$$

where $\beta$ and $\gamma$ are the relativistic beam factors, c is the speed of light, and $\Delta\tau$ is the TOF variation.

Although not listed in this fashion, the resolution is a component of the overall measurement accuracy. As Table II shows, the largest errors are usually linked to the operation and implementation of the measurement (such as electronics noise, alignment, and cable delay errors) and contribute to a majority of the measurement inaccuracies. Although not shown as a problem, radio-frequency interference (RFI) contributions can easily be far greater than those listed in the table. During the early stages of the beam measurement, the RFI noise was as high as -6dBc, which is 25 times greater than that listed in the table – and it effectively rendered most of the beam measurements useless.

## III. CONCLUSIONS

Measurements done with the microstrip probe can provide more information than just the usual beam position and intensity. If two probes with a known, pure drift-distance between them are used, beam angle, energy, and output phase can also be directly measured. These added measurements provide information on the interaction between a beam and an upstream accelerating cavity. The 425-MHz microstrip system developed at Los Alamos initially suffered from RFI-induced errors, but these errors have now been reduced to the point that the measurements provide reliable transverse and longitudinal phase-space beam information.

## IV. REFERENCES


1. R. E. Shafer, "Characteristics of Directional Coupler Position Monitors," IEEE Transaction of Nuclear Science, 32, No. 5, pp. 1933-1937.
2. J. D. Gilpatrick, "Microstrip Probe Impedance Function," AT-3:TN:87-38, 1987.
3. R. B. Shurter, J. D. Gilpatrick, "Tuned Antenna Driver for Microstrip Probe Sensitivity Testing," Workshop on Accelerator Instrumentation, Fermi National Accelerator Lab., Batavia, IL Oct. 1-4, 1990.
4. J. D. Gilpatrick, J. F. Power, F. D. Wells, R. B. Shurter, and R. Meyer, "Overview of the Microstrip Beam Diagnostics," LA-CP-89-460, 1989.
5. J. D. Gilpatrick, J. Power, F. D. Wells, and R. B. Shurter, "Microstrip Probe Electronics," LA-CP-89-488, 1989.
6. J. D. Gilpatrick, R. E. Meyer, F. D. Wells, J. F. Power, and R. E. Shafer, "Synchronous Phase and Energy Measurement System for a 6.7 MeV $H^-$ Beam," 1988 Linear Accelerator Conference, pp. 134-136.
7. K. F. Johnson, O. R. Sander, G. O. Bolme, J. D. Gilpatrick, F. W. Guy, J. H. Marquardt, K. Saadatmand, D. Sandoval, and V. Yuan, "The Single-Beam Funnel Demonstration: Experiment and Simulation," 1990 Linear Accelerator Conference, pp. 701-703.